ORIGINAL PAPER

Determination of xanthine using a ratiometric fluorescence probe based on boron-doped carbon quantum dots and gold nanoclusters

Xuanxuan An[1] · Qin Tan[1] · Shuang Pan[1] · Shujun Zhen[1] · Yongmei Hu[2] · Xiaoli Hu[1]

Abstract

A dual-emission ratiometric fluorescent sensing system based on boron-doped carbon quantum dots (B-CQDs) and gold nanoclusters (AuNCs) has been developed for the determination of xanthine. The blue fluorescence of B-CQDs at 445 nm is then reduced by the AuNCs through the inner filter effect (IFE) under a single excitation wavelength of 370 nm. By the catalysis of xanthine oxidase (XOD), xanthine is oxidized by oxygen dissolved in the solution to produce H_2O_2. The horseradish peroxidase (HRP) catalyzes H_2O_2 to generate hydroxyl radicals, which can quench the fluorescence of AuNCs, leading to the recovery of the fluorescence of B-CQDs. Based on the relationship between the fluorescence intensity ratio (F_{445}/F_{665}) and the concentration of xanthine, the designed method exhibits a good linearity range of 1.2–500.0 μmol L^{-1} and a limit of detection of 0.37 μmol L^{-1}. The ratiometric fluorescent is applied to determine xanthine in human urine samples. Good recoveries of spiked samples in the range 99.2–105.0% are obtained by the proposed assay, with relative standard deviations (RSD) ranging from 0.9 to 2.6%.

Introduction

Xanthine (3,7-dihydropurine-2,6-dione) is a purine derivative produced during the degradation of adenosine triphosphate [1]. It is converted into uric acid under the action of xanthine oxidase (XOD) and widely distributed in the organs and body fluids of humans and other organisms [2]. When there is a lack of XOD, xanthine cannot be converted, resulting in a dramatic increase in the concentration of xanthine in the blood and urine, which can lead to various diseases such as gout, hyperuricemia, and xanthinuria [3–5]. Therefore, the accurate and timely determination of xanthine is of great significance for the diagnosis and monitoring of clinically related diseases. To date, a series of analytical methods have been employed for the detection of xanthine, including electrochemical method [6], colorimetric assays [7], voltammetry [8], high-performance liquid chromatography (HPLC) [9], and fluorimetric method [10, 11]. Among all those methods, as a better method with comparatively low cost, rapid, technical simplicity, and on-site analysis, the fluorimetric method based on luminescent materials serves as a great alternative to detect xanthine.

Because of their excellent properties, such as high light stability, easy synthesis and surface functionalization, adjustable composition and fluorescence emission, good biocompatibility, and low cytotoxicity [12–15], carbon quantum dots (CQDs) are considered to be a promising nanomaterial in chemical and biological sensing, cell imaging, drug delivery and photocatalysis, etc. [16–19]. Benjamin et al. synthesized CQDs using citric acid as a carbon source by hydrothermal method for solar light–driven hydrogen production in aqueous solution [20]. However, the quantum yield of carbon dots synthesized from a single carbon source was low, only 1.4%. Heteroatom doped (nitrogen, sulfur, phosphorus and boron, etc.) can adjust the carbon frameworks and their surface chemical structures to create new excited energy potentials, thus improving the fluorescence quantum

✉ Yongmei Hu
huyongmei2000@163.com

✉ Xiaoli Hu
xiaolihu@swu.edu.cn

[1] Key Laboratory of Luminescence Analysis and Molecular Sensing, Ministry of Education, College of Chemistry and Chemical Engineering, Southwest University, Chongqing 400715, People's Republic of China

[2] Chengdu Second People's Hospital, Chengdu 610017, People's Republic of China
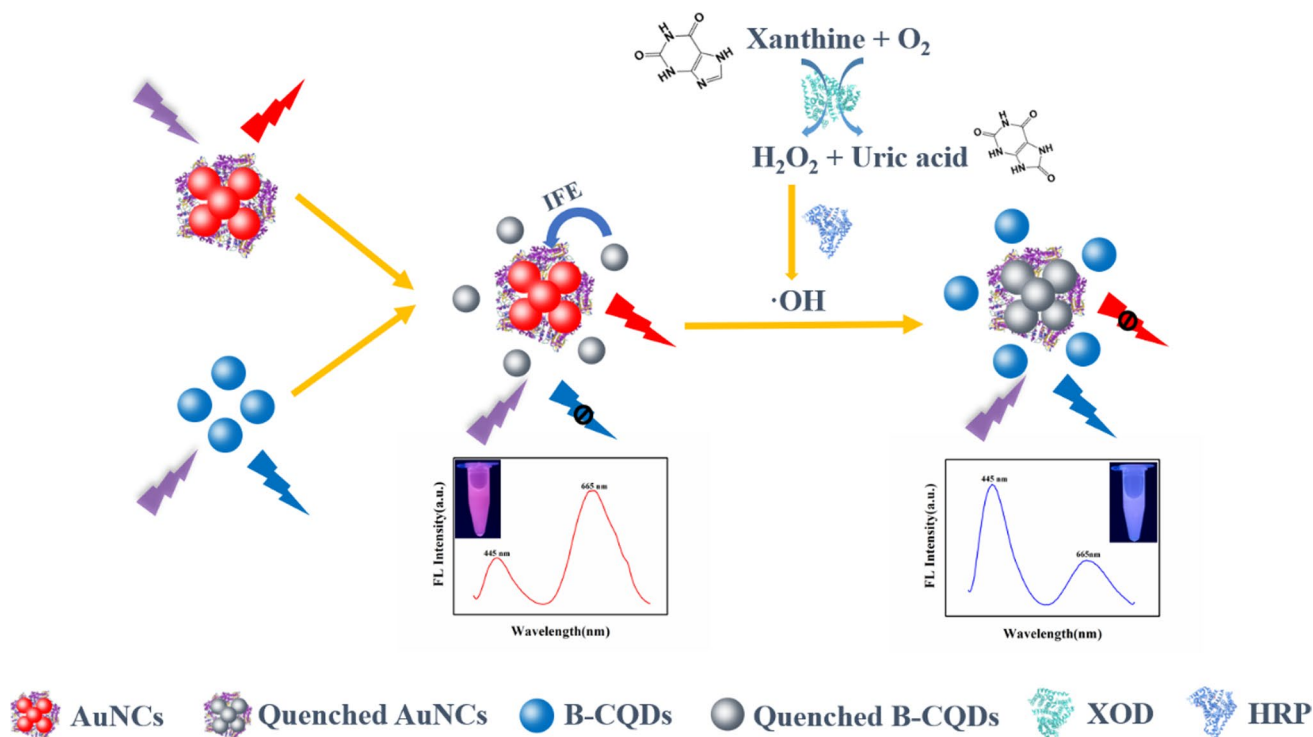
Scheme 1 Schematic diagram of the mechanism of xanthine detection in B-CQDs and AuNCs sensing system.

yields and inherent properties of the CQDs. In particular, the doping of CQDs with B atom effectively regulates the electronic and optical properties of the CQDs because the vacant p-orbital of B atom can effectively conjugate with C=C, thus decreasing the distance between B(III) and the sp^2 clusters of CQDs, which could enhance the electronic delocalization in the carbon matrix [21, 22]. For example, Ma et al. used citric acid and sodium tetraphenylborate as raw materials to synthesize boron-doped carbon quantum dots (B-CQDs) (quantum yield 42%) by the hydrothermal method as a fluorescent probe, achieving the ultrasensitive sensing of catechol and glutathione [23].

However, the quantitative analysis of targets using fluorescent probes with a single emission characteristic will be interfered by various factors unrelated to the analyte (such as instrumental parameters, the microenvironment surrounding and local concentration of probe molecules, and photobleaching) [24]. In order to overcome these problems and ensure reliability, an effective strategy is to design a dual-emission ratiometric scheme by introducing another fluorescence spectrum peak. Ideally, a ratiometric fluorescence probe harvests the target-induced fluorescence intensity changes from two or more emission bands at different wavelengths. The obtained signal ratio can reduce the interference with environment/background factors to the greatest extent, so as to realize the reliable detection of specific targets [25]. Zhao et al. designed a ratiometric fluorescence probe based

on CQDs and gold nanoclusters (AuNCs) for the sensitive detection of hydrogen peroxide (H_2O_2). The change of the ratiometric fluorescence signal depends on how ferrous ion reacts with H_2O_2 to produce hydroxy radicals ($\cdot OH$) and hydroperoxy radicals ($\cdot OOH$) [26].

Here, we reported a ratiometric fluorescent sensing system based on B-CQDs and AuNCs for the determination of xanthine (Scheme 1). Firstly, AuNCs quenched the blue fluorescence of B-CQDs through the inner filter effect (IFE) under a single excitation wavelength of 370 nm. Then, xanthine oxidase (XOD) catalyzed xanthine to produce H_2O_2 and uric acid. Furthermore, H_2O_2 was catalyzed by horseradish peroxidase (HRP) to generate $\cdot OH$ that quenched the red fluorescence of AuNCs, leading to recovery of the blue fluorescence of B-CQDs. This method was also successfully applied to the determination of xanthine in human urine samples.

Experimental section

Materials

Xanthine, horseradish peroxidase (HRP), bovine serum albumin (BSA), and polyethyleneimine (PEI, M.W.600) were purchased from Aladdin Chemistry Co. Ltd. (Shanghai, China). Chloroauric acid was gained from Nanjing reagent

(Nanjing, China). Xanthine oxidase (XOD) was obtained from Macklin Biochemical Co. Ltd. (Shanghai, China). Citric acid monohydrate and boric acid were gained from Oriental Reagent Factory (Chongqing, China). All reagents were of analytical grade and the water used in the work was deionized water.

Instruments

The UV-2700 spectrophotometer (Hitachi, Tokyo, Japan) was used to measure the absorption spectra and absorbance. The F-2500 spectrofluorometer from Hitachi was used to obtain fluorescence spectra and intensity. Transmission electron microscope (TEM) images of B-CQDs and AuNCs were obtained using a Hitachi S-4800 scanning electron microscope (Tokyo, Japan). Fourier transform infrared spectrum (FI-TR) was conducted on a FTIR-8400S FTIR spectrometer. The X-ray diffraction (XRD) patterns were given from a X-ray diffractometer (Rigaku D/MAX 2550). The chemical composition of the products was examined with X-ray photoelectron spectrometer (XPS) from Escalab 250Xi (Thermo Fisher Scientific, USA). Zeta potentials were measured by dynamic laser light scattering (ZEN3690, Malvern).

Synthesis of B-CQDs and AuNCs

The B-CQDs and AuNCs were prepared according to previously reported study with minor modifications [23, 27]. Specific synthesis methods were described in the Supporting information.

Detection of xanthine

Typically, 100.0 μL of phosphate buffer (0.2 mol L^{-1}, pH 6.4), 100.0 μL of xanthine at varying concentrations, 50.0 μL XOD (100 μg/mL), and 30.0 μL HRP (50 μg/mL) were mixed to produce ·OH. After that, 100.0 μL of AuNCs, 50.0 μL B-CQDs, and 570.0 μL of deionized water were added into the mixture and incubated for 50 min at 37 °C. Finally, the fluorescence emission spectrum of the whole solution was measured under the excitation wavelength of 370 nm. The fluorescence intensity at the emission wavelengths of 445 nm and 665 nm was recorded.

Real sample assay

The human urine samples were obtained from three healthy volunteers in the Chengdu Second People's Hospital. The sample analysis experimental protocol was approved by the institutional committee of Chengdu Second People's Hospital (approval number 2021088), and all the guidelines were followed throughout the present study. These samples were first treated by adding $BaCl_2$ (0.1 mol L^{-1}) and $ZnSO_4$ (0.1

mol L^{-1}) and centrifuged at 10,000 rpm for 5 min to remove protein. Then, the supernatants were filtered through a 0.22-μm membrane, and the filtrates were collected for determination. Different concentrations of xanthine were spiked into the urine sample and recovery experiments were performed. The specific method was as follows: 500.0 μL of sample solution was mixed with 100.0 μL of standard xanthine solution at different concentrations (2.0, 250.0, and 400.0 μmol L^{-1}). Finally, the treated sample was added into 100.0 μL of phosphate buffer (0.2 mol L^{-1}, pH 6.4), and was detected by the method described above.

Results and discussion

Characterization of B-CQDs and AuNCs

Fig. 1a revealed that the B-CQDs were uniform spheres with an average diameter of ~3.73 nm. Besides, HR-TEM image disclosed its good crystallization nature, showing a lattice spacing of ~0.25 nm, corresponding to the in-plane lattice spacing of graphene (100). The AFM image (Fig. 1b) also gave the spherical morphologies of the B-CQDs particles, where the heights were in the range of −1 to 3nm. Other characterization results of B-CQDs were described in detail in the Supporting information. The XRD, FRIT, and XPS characterizations of B-CQDs are displayed in Supplementary Fig. S1. All the results illustrated the successful synthesis of B-CQDs. As is illustrated in Fig. 1c, the modality and the average particle size of AuNCs were characterized by TEM, indicating that as-prepared AuNCs were uniformly spherical with the sizes ranging from 0.52 to 3.19 nm, together with an average size of 1.42 nm. Besides, the HR-TEM image disclosed the crystal lattice fringes with an interplanar spacing distance of 0.24 nm corresponding to the (1 1 1) crystal planes of the face-centered cubic Au [28]. The XRD and XPS characterizations of AuNCs are displayed in Supplementary Fig. S2. Moreover, the optical properties of the B-CQDs and AuNCs have been described in Supplementary Fig. S3.

Feasibility analysis and mechanism discussion

As is illustrated in Fig. 2a, the fluorescence of B-CQDs at 445 nm was reduced after adding AuNCs. The ratiometric fluorescence of the system did not have an obvious change in the presence of xanthine and HRP individually. However, with the addition of xanthine, XOD, and HRP at the same time, the fluorescence intensity of AuNCs decreased, while the fluorescence intensity of the B-CQDs recovered. In addition, it can be seen from the UV-Vis absorption spectrum in Fig. 2b that AuNCs reduced the absorbance of B-CQDs at 360 nm. When xanthine, XOD, and HRP were added to the fluorescence

Fig. 1 **a** TEM image of B-CQDs (inset: HR-TEM image and particle size distribution histogram). **b** AFM image of B-CQDs. **c** TEM image of AuNCs (inset: HR-TEM images and particle size distribution histogram).
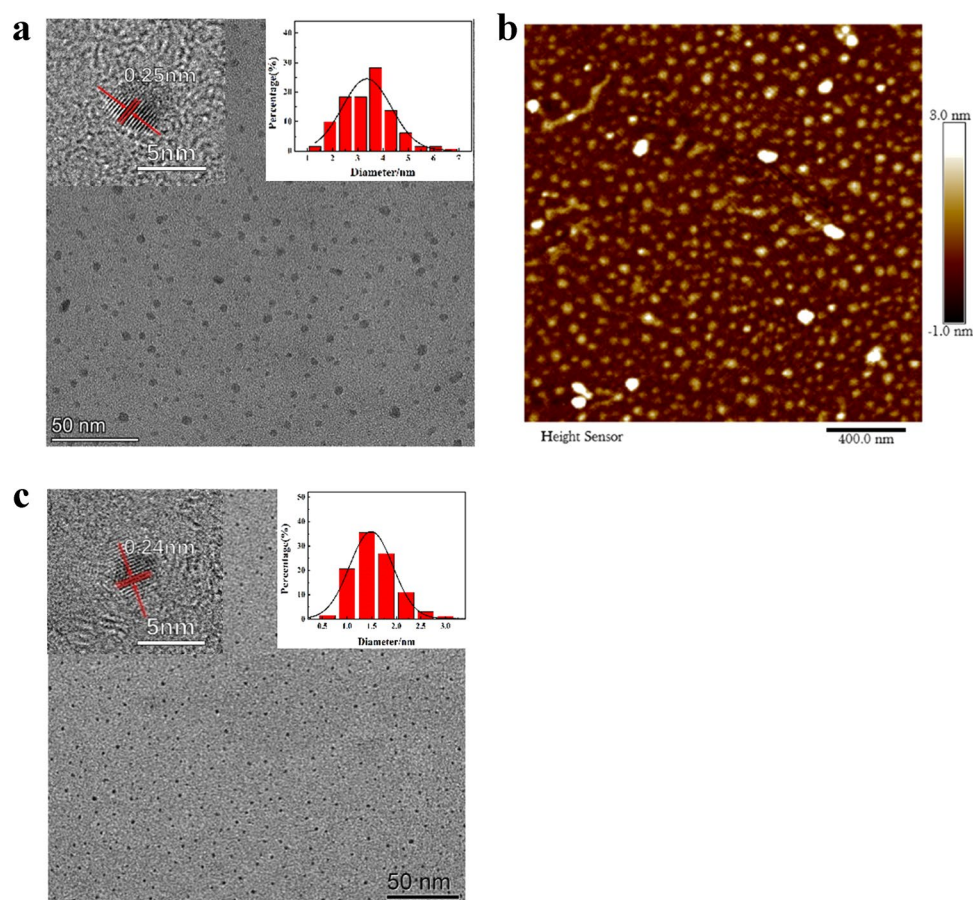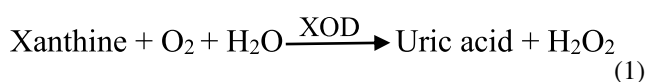

Fig. 2 **a** The fluorescence spectra of B-CQDs, AuNCs, B-CQDs + AuNCs, B-CQDs + AuNCs + xanthine, B-CQDs + AuNCs + HRP, B-CQDs+ AuNCs + xanthine + XOD and B-CQDs + AuNCs + xanthine + XOD + HRP. **b** The UV-Vis absorption spectrum of B-CQDs, AuNCs, B-CQDs + AuNCs, B-CQDs + AuNCs + xanthine + XOD and B-CQDs + AuNCs + xanthine + XOD + HRP. **c** The fluorescence spectra of B-CQDs and the UV-Vis absorption spectra of AuNCs. **d** The fluorescence decay curves of B-CQDs and B-CQDs + AuNCs.
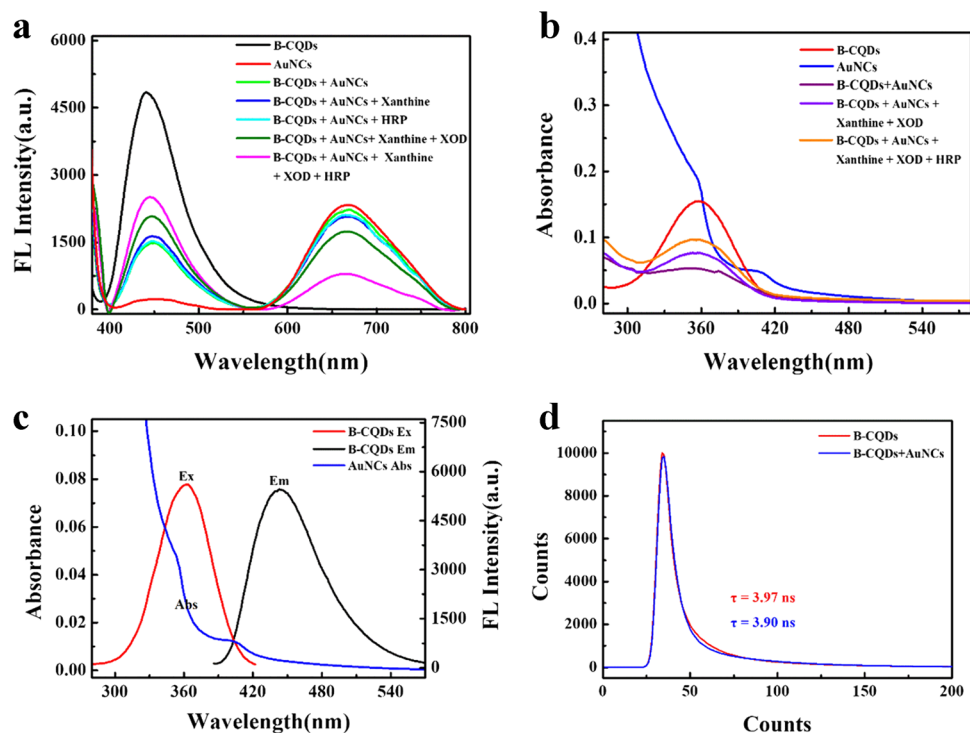
system, the absorbance of the B-CQDs was recovered obviously. These results demonstrated that the designed ratiometric fluorescent sensing system was feasible.

Actually, xanthine was catalyzed by XOD to produce H_2O_2 and uric acid (Eq. (1)) [7, 10]. Then, HRP catalyzed H_2O_2 to generate ·OH that quenched the fluorescence of AuNCs. As shown in Supplementary Fig. S4, the fluorescence quenching of AuNCs was more obvious after adding HRP, because ·OH can afford stronger oxidation capacity than H_2O_2. The possible reason for fluorescence quenching of AuNCs was assigned to the powerful oxidation ability of ·OH [26, 29]. As shown in Fig. 2b, after the addition of xanthine, XOD, and HRP to produce ·OH, the weak absorption peaks of AuNCs at about 420 nm disappeared. Therefore, ·OH could partially dissolve the AuNCs and lead to the recovery of the fluorescence of B-CQDs.

$$\text{Xanthine} + O_2 + H_2O \xrightarrow{\text{XOD}} \text{Uric acid} + H_2O_2 \tag{1}$$

To investigate the mechanism of the fluorescence of B-CQDs quenched by AuNCs, the relevant experiments were carried out. It can be seen from Fig. 2c that the fluorescence spectra of the B-CQDs were effectively overlapped by the UV-Vis absorption spectrum of AuNCs. Additionally, no new absorption peak appeared in the UV-Vis absorbance spectrum of the B-CQDs-AuNCs system, indicating that a new complex was not formed in Fig. 2b. Therefore, the mechanism by which the fluorescence of B-CQDs was quenched by AuNCs may be fluorescence resonance energy transfer (FRET) or inner filter effect (IFE). As can be seen from Fig. 2d, the fluorescence lifetimes of the B-CQDs and the B-CQDs-AuNCs were calculated to be 3.97 ns and 3.90 ns, respectively. According to the well-known equation for evaluation of FRET efficiency [30]:

$$E = 1 - \tau_{D-A}/\tau_D \tag{2}$$

Here, E is the energy transfer efficiency, τ_D and τ_{D-A} are fluorescence lifetimes of the donor and the donor-acceptor pair, respectively. The FRET efficiency of the B-CQDs-AuNCs composite was calculated to be 1.7%. The calculated

FRET efficiency was in disagreement with the observed fluorescence quenching efficiency (61.3%, Fig. 2a). Besides, as shown in Supplementary Fig. S5, the Zeta potentials of B-CQDs, AuNCs, and the mixture were −0.46, −1.91, and −5.31 mV, all of which were negatively charged, indicating that there was electrostatic repulsion between B-CQDs and AuNCs. Therefore, B-CQDs and AuNCs cannot be close to produce FRET [31]. Above all, the possible mechanism for the fluorescence of B-CQDs quenched by AuNCs could be primarily owing to IFE.

Optimization of experimental parameters

Firstly, the ratiometric fluorescence of CQDs-AuNCs system was barely affected by different concentrations of NaCl solution, radiation time, and pH (Fig. S6), which proved that the system was relatively stable. Furthermore, in order to achieve better experimental result, the incubation time, pH, and the concentration of XOD and HRP were optimized. Respective data and figures are given in Supplementary Fig. S7. It was found that the following experimental conditions got the best results: (a) the reaction reached equilibrium after 50 min; (b) pH 6.4; (c) 50.0 μL of 100 μg mL^{-1} XOD; (d) 30.0 μL of 50 μg mL^{-1} HRP.

Ratiometric fluorescence detection of xanthine

The feasibility of the detection system was studied by the fluorescence enhancing of B-CQDs and quenching of AuNCs, with different concentrations of xanthine under optimum experimental conditions. Fig. 3a clearly showed that the blue fluorescence of the CQDs at 445 nm gradually increased, whereas the red fluorescence of AuNCs decreased at 665 nm under the 370-nm excitation wavelength with the increase of the concentrations of xanthine from 0 to 500 μmol L^{-1}. As shown in Fig.3b, a good linear relationship of F_{445}/F_{665} with concentration of xanthine was obtained. The linear regression equation was $F_{445}/F_{665} = 0.0034C + 1.04$ ($R^2 = 0.997$). The limit of detection (LOD) was evaluated to be 0.37 μmol L^{-1} based on the formula LOD $= 3\sigma/k$ and the

Fig. 3 **a** Ratiometric fluorescence spectra of various concentrations of xanthine from 0 to 500.0 μmol L^{-1}. **b** The linear of F_{445}/F_{665} with different concentrations of xanthine (0.5–500.0 μmol L^{-1}).
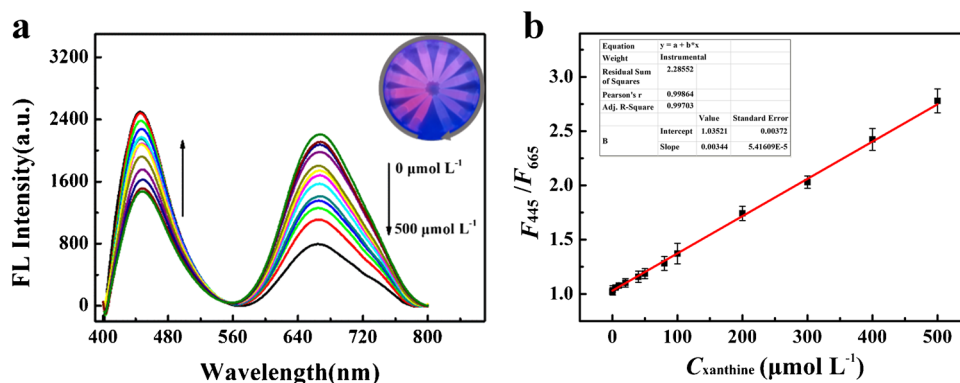
limit of quantitation (LOQ) was calculated to be 1.2 µmol L^{-1} based on the formula LOQ = 10σ/k. Thus, this method had a linear range of 1.2–500.0 µmol L^{-1}. Table 1 exhibited a ratiometric fluorescence probe based on CQDs and AuNCs and other probes for the determination of xanthine. Compared with colorimetry [7] and voltammetry [8], the ratiometric fluorescence probe manifested a relatively wide detection range and the low LOD. Compared with single-signal electrochemical [6] and fluorescence method [11], etc., a dual-emission fluorescent probe could decrease or eliminate the errors caused by the fluctuations in environmental/testing conditions. Additionally, compared with other methods, the proposed method had the widest linear range.

In order to evaluate the anti-interference ability of the present method towards xanthine, the fluorescence response of the system after the addition of possible interfering substances was recorded. Furthermore, it was mainly to select inorganic salts, amino acids, uric acid, and urea, as well as substances similar in structure to xanthine as interferences. The concentration of the interferences was selected based on the concentration ratio of the main interferences and the target analyte in human urine sample [32]. As depicted in Table 2, interferences could be able to co-exist with xanthine with a relative error under 5.0%. The results confirmed that the established method possessed good selectivity and strong anti-interference capability for the detection of xanthine.

Determination of xanthine in real samples

In order to verify the actual availability of the ratiometric fluorescent probe, different concentrations of xanthine were spiked into the human urine samples and recovery experiments were performed. The concentration of xanthine in the urine sample was measured by HPLC method [33]. The ratiometric fluorescence method was used to measure the total concentration in the real sample with addition of the standard solution of xanthine. The choice of the analyte concentrations referred to an official website (https://www.fda.gov/home). Official guidelines suggested that the concentration of analyte added to the real sample depended on the linear range. The upper limit, lower limit, and middle value close to the linear range were selected as the analyte concentrations. Hence, 2.0, 250.0, and 400.0 µmolL^{-1} were selected as the concentrations of xanthine in the spiked experiment. Comparisons of the determination results by our method and the HPLC method are shown in Table 3. The concentration of xanthine was found to be 1.7±0.2 µmol L^{-1} in human urine sample by the HPLC method. In addition, good recoveries of spiked experiment in the range of 99.2–105.0% were obtained by the proposed assay, with the relative standard deviations (RSD) ranging from 0.9 to 2.6%. These results indicated that the determination results of established method were very close to the value through the

Table 1 Comparison of linear range and detection limit of various methods for xanthine detection.

Analytical methods	Materials	Linear range (µmol L^{-1})	Detection limit (µmol L^{-1})	Reference
Electrochemistry	Chitosan/PPy/Au-NPs	1.0–100.0	0.10	[6]
Colorimetry	WO_3 nanosheets	25.0–200	1.24	[7]
Voltammetry	Pt@MIL-101(Cr)	0.5–162.0	0.42	[8]
Fluorescence	SiNPs	0.3–200.0	0.11	[11]
Fluorescence	AuNCs/B-CQDs	1.2–500.0	0.37	This work

Table 2 Effects of coexisting substances ($C_{xanthine}$ =2.0 µmol L^{-1}=0.3 µg mL^{-1}).

Species	Concentration (µg mL^{-1})	Relative error (%)	Species	Concentration (µg mL^{-1})	Relative error (%)
NaCl	212.8	−3.3	Uric acid	7.1	1.2
$MgCl_2$	5.1	−2.6	Dopamine	3.1	-2.1
$CaCl_2$	1.2	−0.4	Adenosine	5.4	1.2
KCl	126.7	−1.0	Theophylline	3.6	2.3
$FeSO_4$	0.6	0.6	Sucrose	6.8	1.7
$CuSO_4$	0.3	3.7	Guanine	0.3	-0.2
Glucose	3.6	−3.1	Urea	1.5	2.6
Glutathione	6.3	−1.1	Oxalic acid	1.5	-3.6
Cysteine	2.4	−1.8	Alanine	1.9	3.0
Ascorbic acid	3.5	−1.9	Glycine	22.8	0.7
6-Mercaptopurine	2.4	−0.1	DL-Lysine	2.8	-1.5

Table 3 Recoveries for the determination of xanthine in human urine sample ($n = 3$).

Sample	Add (μmolL^{-1})	Found ±SD (μmol L^{-1})	Recovery (%)	RSD (%)
1	0	$1.7 \pm 0.2^*$	--	11.8
2	2.0	3.8 ± 0.1	105.0	2.6
3	250.0	253.1 ± 2.2	100.6	0.9
4	400.0	398.5 ± 6.1	99.2	1.5

* Tested by the HPLC method

SD standard deviation

HPLC method. Therefore, this method may be potentially applied for the screening and determination of xanthine in human urine sample.

However, this established method had some limitations in a real assay. One disadvantage of the method was working in the UV made the probe prone to interferences by biomolecules. The UV absorption and fluorescence signals may be interfered with by blood, serum, cells, seawater, etc. Therefore, the urine sample was centrifuged to remove protein and further purified through the filter membrane to reduce the interference on working in the UV.

Conclusion

In this work, a ratiometric fluorescent probe based on B-CQDs and AuNCs was designed for sensitive and selective the determination of xanthine. The functionalized boron-doped CQDs were successfully prepared by the one-pot hydrothermal method. The B-CQDs emitting blue light at 445 nm were quenched by the AuNCs due to IFE. By the catalysis of XOD, xanthine was oxidized by oxygen dissolved in the solution to produce H_2O_2. Then, H_2O_2 was catalyzed by HRP to generate $\cdot$OH, which could quench the fluorescence of the AuNCs, thus recovering the fluorescence of B-CQDs. According to the change of the ratiometric fluorescence signal, the quantitative determination of xanthine was finally realized. Because of the specific combination of xanthine and XOD, the selectivity of this probe was greatly improved. In addition, this method had been successfully used for the determination of xanthine in human urine samples, indicating its potential application prospects in clinical testing.

Declarations

References

1. Dervisevic M, Dervisevic E, Senel M (2019) Recent progress in nanomaterial-based electrochemical and optical sensors for hypoxanthine and xanthine. A review Microchimica Acta 186(12):749–773. https://doi.org/10.1007/s00604-019-3842-6

2. Kant R, Tabassum R, Gupta BD (2018) Xanthine oxidase functionalized Ta_2O_5 nanostructures as a novel scaffold for highly sensitive SPR based fiber optic xanthine sensor. Biosens Bioelectron 99:637–645. https://doi.org/10.1016/j.bios.2017.08.040

3. Karissa YK, Ralph SH, Elke H, Albert IW, Sheldon XK (2003) A literature review of the epidemiology and treatment of acute gout. Clin Ther 25:1593–1617. https://doi.org/10.1016/s0149-2918(03)80158-3

4. Campion EW, Glynn RJ, DeLabry LO (1987) Asymptomatic hyperuricemia. Risks and consequences in the Normative Aging Study. Am J Med 82:421–426. https://doi.org/10.1016/0002-9343(87)90441-4

5. Kawachi M, Kono N, Mineo I, Y Yamada Y, Tarui S (1990) Decreased xanthine oxidase activities and increased urinary oxypurines in heterozygotes for hereditary xanthinuria. Clin Chim Acta 188:137-146. https://doi.org/10.1016/0009-8981(90)90158-o

6. Dervisevic M, Dervisevic E, Cevik E, Senel M (2017) Novel electrochemical xanthine biosensor based on chitosan-polypyrrole-gold nanoparticles hybrid bio-nanocomposite platform. J Food Drug Anal 25(3):510–519. https://doi.org/10.1016/j.jfda.2016.12.005

7. Li Z, Liu X, Liang XH, Zhong J, Guo L, Fu F (2019) Colorimetric determination of xanthine in urine based on peroxidase-like activity of WO_3 nanosheets. Talanta 204:278–284. https://doi.org/10.1016/j.talanta.2019.06.003

8. Zhang L, Li S, Xin J, Ma H, Pang H, Tan L et al (2018) A non-enzymatic voltammetric xanthine sensor based on the use of platinum nanoparticles loaded with a metal-organic framework of type MIL-101(Cr). Application to simultaneous detection of dopamine, uric acid, xanthine and hypoxanthine. Microchim Acta 186(1):1–10. https://doi.org/10.1007/s00604-018-3128-4

9. Kock R, Delvoux B, Greiling H (1993) A high-performance liquid chromatographic method for the determination of hypoxanthine, xanthine, uric acid and allantoin in serum. European journal of clinical chemistry and clinical biochemistry: journal of the Forum of European 31:303–310

10. Wang L, Liu Y, Yang Z, Wang Y, Rao H, Yue G et al (2020) A ratiometric fluorescence and colorimetric dual-mode assay for H_2O_2 and xanthine based on Fe, N co-doped carbon dots. Dyes Pigments 180:108486–108493. https://doi.org/10.1016/j.dyepig.2020.108486

11. Li D, Chen F, Li N, Ye X, Sun Y, Ma P et al (2021) Sensitive ratiometric fluorescence assay for detecting xanthine in serum based on the inner filter effect of enzyme-catalyzed oxidation products to silicon nanoparticles. Anal Bioanal Chem 413(5):1405–1415. https://doi.org/10.1007/s00216-020-03104-7

12. Lim SY, Shen W, Gao Z (2015) Carbon quantum dots and their applications. Chem Soc Rev 44(1):362–381. https://doi.org/10.1039/C4CS00269E

13. Molaei MJ (2020) The optical properties and solar energy conversion applications of carbon quantum dots: a review. Sol Energy 196:549–566. https://doi.org/10.1016/j.solener.2019.12.036

14. Li Q, Ohulchanskyy TY, Liu RL, Koynov K, Wu DQ, Best A, Kumar R, Bonoiu A, Prasad PN (2010) Photoluminescent carbon dots as biocompatible nanoprobes for targeting cancer cells in vitro. J Phys Chem C 114:12062–12068. https://doi.org/10.1021/jp911539r

15. Huang YF, Zhou R, Zhang H, Kang KB, Zhao M, Peng Y, Wang Q, Zhang HL, Qiu WY (2014) One-pot synthesis of highly luminescent carbon quantum dots and their nontoxic ingestion by zebrafish for in vivo imaging. Chem Eur J 20(19):5640–5648. https://doi.org/10.1002/chem.201400011

16. Zhu S, Meng Q, Wang L, Zhang J, Song Y, Jin H et al (2013) Highly photoluminescent carbon dots for multicolor patterning, sensors, and bioimaging. Angew Chem Int Ed 52(14):4045–4049. https://doi.org/10.1002/anie.201300519

17. Alexander LA, Joshua TR, Omar KY, Hong GS, Diao S, Richard L, Dai HJ (2013) Ultra-low doses of chirality sorted (6,5) carbon nanotubes for simultaneous tumor imaging and photothermal therapy. ACS Nano 7(4):3644–3652. https://doi.org/10.1021/nn4006472

18. Feng T, Ai X, An G, Yang P, Zhao Y (2016) Charge-convertible carbon dots for imaging-guided drug delivery with enhanced in vivo cancer therapeutic efficiency. ACS Nano 10(4):4410–4420. https://doi.org/10.1021/acsnano.6b00043

19. Li H, He X, Kang Z, Huang H, Liu Y, Liu J et al (2010) Water-soluble fluorescent carbon quantum dots and photocatalyst design. Angew Chem Int Ed 49(26):4430–4434. https://doi.org/10.1002/anie.200906154

20. Martindale BCM, Hutton GAM, Caputo CA, Reisner E (2015) Solar hydrogen production using carbon quantum dots and a molecular nickel catalyst. J Am Chem Soc 137(18):6018–6025. https://doi.org/10.1021/jacs.5b01650

21. Sadhanala HK, Pagidi S, Gedanken A (2021) High quantum yield boron-doped carbon dots: a ratiometric fluorescent probe for highly selective and sensitive detection of Mg^{2+} ions. J Mater Chem C 9(5):1632–1640. https://doi.org/10.1039/D0TC05081D

22. Wang F, Hao Q, Zhang Y, Xu Y, Lei W (2015) Fluorescence quenchometric method for determination of ferric ion using boron-doped carbon dots. Microchim Acta 183(1):273–279. https://doi.org/10.1007/s00604-015-1650-1

23. Ma Y, Chen AY, Huang YY, He X, Xie XF, He B et al (2020) Off-on fluorescent switching of boron-doped carbon quantum dots for ultrasensitive sensing of catechol and glutathione. Carbon 162:234–244. https://doi.org/10.1016/j.carbon.2020.02.048

24. Zhang Z, Feng J, Huang P, Li S, Wu FY (2019) Ratiometric fluorescent detection of phosphate in human serum with functionalized gold nanoclusters based on chelation-enhanced fluorescence. Sensors Actuators B Chem 298:126891–126896. https://doi.org/10.1016/j.snb.2019.126891

25. Huang X, Song J, Yung BC, Huang X, Xiong Y, Chen X (2018) Ratiometric optical nanoprobes enable accurate molecular detection and imaging. Chem Soc Rev 47(8):2873–2920. https://doi.org/10.1039/C7CS00612H

26. Zhao Q, Zhou C, Yang Q, Chu Z, Jia N (2019) A FRET-based fluorescent probe for hydrogen peroxide based on the use of carbon quantum dots conjugated to gold nanoclusters. Microchim Acta 186(5):294–301. https://doi.org/10.1007/s00604-019-3398-5

27. Xie JP, Zheng YG, Ying JY (2009) Protein-directed synthesis of highly fluorescent gold nanoclusters. J Am Chem Soc 131:888–889. https://doi.org/10.1021/ja806804u

28. Sun J, Yue Y, Wang P, He H, Jin Y (2013) Facile and rapid synthesis of water-soluble fluorescent gold nanoclusters for sensitive and selective detection of Ag^+. J Mater Chem C 1(5):908–913. https://doi.org/10.1039/C2TC00207H

29. Wen F, Dong Y, Feng L, Wang S, Zhang S, Zhang X (2011) Horseradish peroxidase functionalized fluorescent gold nanoclusters for hydrogen peroxide sensing. Anal Chem 83(4):1193–1196. https://doi.org/10.1021/ac1031447

30. Algar WR, Kim HM, Igor L, Hildebrandt N (2014) Emerging non-traditional Förster resonance energy transfer configurations with semiconductor quantum dots: Investigations and applications. Coord Chem Rev 263-264:65–85. https://doi.org/10.1016/j.ccr.2013.07.015

31. Yuan L, Lin WY, Zheng KB, Zhu SS ((201)) FRET-based small-molecule fluorescent probes: rational design and bioimaging applications. Acc Chem Res 46(7):1462–1473. https://doi.org/10.1021/ar300273v

32. Urine analysis, Guangdong Science and Technology Press, Guangzhou, 1980, 8-11

33. Harkness RA (1988) Hypoxanthine, xanthine and uridine in body fluids, indicators of ATP depletion. J Chromatogr 429:255–278. https://doi.org/10.1016/s0378-4347(00)83873-6